

Modeling Active Non-Markovian Oscillations

G. Tucci^{1,*}, É. Roldán^{2,†}, A. Gambassi^{1,‡}, R. Belousov^{2,3,§}, F. Berger⁴, R. G. Alonso⁵, and A. J. Hudspeth⁵


¹SISSA—International School for Advanced Studies and INFN, via Bonomea 265, 34136 Trieste, Italy

²ICTP—The Abdus Salam International Centre for Theoretical Physics, Strada Costiera 11, 34151 Trieste, Italy

³EMBL—European Molecular Biology Laboratory, Meyerhofstrasse 1, 69117 Heidelberg, Germany

⁴Cell Biology, Neurobiology and Biophysics, Department of Biology, Faculty of Science, Utrecht University, 3584 CH Utrecht, Netherlands

⁵Howard Hughes Medical Institute and Laboratory of Sensory Neuroscience, The Rockefeller University, 1230 York Avenue, New York, New York 10065, USA

 (Received 7 March 2022; accepted 10 June 2022; published 14 July 2022)

Modeling noisy oscillations of active systems is one of the current challenges in physics and biology. Because the physical mechanisms of such processes are often difficult to identify, we propose a linear stochastic model driven by a non-Markovian bistable noise that is capable of generating self-sustained periodic oscillation. We derive analytical predictions for most relevant dynamical and thermodynamic properties of the model. This minimal model turns out to describe accurately bistablelike oscillatory motion of hair bundles in bullfrog sacculus, extracted from experimental data. Based on and in agreement with these data, we estimate the power required to sustain such active oscillations to be of the order of 100 $k_B T$ per oscillation cycle.

DOI: [10.1103/PhysRevLett.129.030603](https://doi.org/10.1103/PhysRevLett.129.030603)

Most nonequilibrium systems *actively* sustain their dynamics by dissipating energy into their environment and by producing entropy, as observed in several branches of natural sciences [1–12]. Important examples are “active oscillators,” the effective mesoscopic degrees of freedom of which are described by oscillating variables. In nature, these oscillators drive climate changes, sustain heart beat, facilitate vocal and auditory systems, and support neural signaling and circadian rhythms [1,4,13–34]. Here we focus on those responsible for mechano-electrical transduction in the bullfrog’s sacculus, for which experimental data are available [4,13,14].

Active oscillatory motion is often interpreted as relaxation oscillations or noisy bistable oscillations, which can be modeled by stochastic Van der Pol and Duffing equations [4,13–33,35,36], respectively. These two distinct dynamical regimes are not always easy to distinguish in experiments. An alternative way to construct a system displaying bistable oscillations consists of letting one of its degrees of freedom to be a two-state stochastic process such as telegraph noise [37–45].

In this Letter, we propose a stochastic linear model for self-sustained, active, bistable oscillations. The model generalizes the Ornstein-Uhlenbeck process by allowing the equilibrium position (the center of the harmonic potential) to be determined by a dichotomous non-Markovian noise. Notably, depending on the distributions of the waiting times, the model can reproduce a wide variety of bistable oscillations, including Markovian and non-Markovian switching processes. We obtain exact analytical predictions for several

dynamical and thermodynamic quantities characterizing the nonequilibrium nature of the system. As a relevant application, we use our model to reproduce recordings of the spontaneous motion in bullfrog hair bundles and estimate the dissipated power, which is experimentally inaccessible but crucial for interpreting the energetics of system.

Model.—We consider an Ornstein-Uhlenbeck process $x(t)$ with time-dependent center $c(t)$ described by the stochastic differential equation

$$\gamma \dot{x}(t) = -\kappa[x(t) - c(t)] + \xi(t). \quad (1)$$

Here κ is the stiffness of the harmonic potential $V(x, c) = \kappa(x - c)^2/2$, γ is the effective friction coefficient, and $\xi(t)$ is a Gaussian white noise with zero mean $\langle \xi(t) \rangle = 0$ and autocorrelation $\langle \xi(t_1) \xi(t_2) \rangle = 2\gamma^2 D \delta(t_1 - t_2)$, where the effective diffusion coefficient $D = k_B T / \gamma$ is related to the temperature through the Einstein relation. The center $c(t)$ is a dichotomous process taking the values $\pm c_0$, with $c_0 \geq 0$, and changing sign at stochastic intervals. We denote by $\psi_{\pm}(\tau)$ the distribution of the waiting time spent in $\pm c_0$ before switching sign; we refer to Fig. 1(a) for an illustration. The relevant timescales of the dynamics are the two mean waiting times $\langle \tau \rangle_{\pm} \equiv \int_0^{\infty} d\tau \tau \psi_{\pm}(\tau)$ and the relaxation time $\tau_{\nu} = \nu^{-1}$ in the harmonic potential, where $\nu = \kappa/\gamma$. Note that $c(t)$ is a non-Markovian process unless the two waiting-time distributions are exponential $\psi_{\pm}(\tau) = e^{-\tau/\langle \tau \rangle_{\pm}} / \langle \tau \rangle_{\pm}$. In this case, $c(t)$ corresponds to the so-called (Markovian) telegraph noise [46].

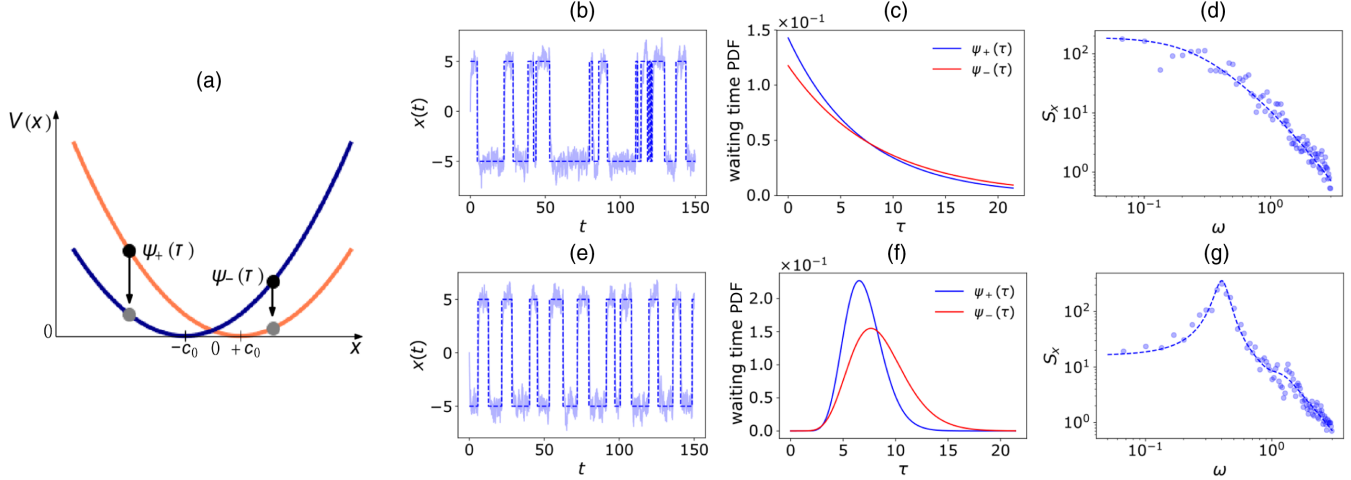


FIG. 1. (a) Schematic representation of the switching mechanism controlling the dynamics described in Eq. (1): after a time τ drawn from the distribution $\psi_{\pm}(\tau)$ the center c of a harmonic potential $V(x) = (\kappa/2)(x - c)^2$ switches from $\pm c_0$ to $\mp c_0$. (b), (e) Realizations of the stochastic driving $c(t)$ (dashed blue line) and of the process $x(t)$ (solid blue line) obtained from a numerical simulation of Eq. (1), for (b) the exponential and (e) the gamma waiting-time probability density function (PDF) plotted, respectively, in (c) and (f). In particular, the exponential distributions have rates $r_+ = 1/7$ and $r_- = 2/17$, whereas the gamma distributions (see the main text) have shape parameters $k_+ = 15$, $k_- = 10$, and scale parameters $\theta_+ = 7/15$, $\theta_- = 17/20$. (d), (g) Power spectral density S_x (symbols) of $x(t)$ on the doubly logarithmic scale, obtained for two time series of total duration $t = 1.5 \times 10^3$ with the same parameters as those in (b) and (e). The dashed lines are given by Eq. (6). The dynamics was simulated with $D = 1$, $c_0 = 5$, $\nu = 2.5$, and a time step $\Delta t = 10^{-3}$.

In Fig. 1 we compare representative trajectories of the process $x(t)$ for various choices of the waiting-time distributions $\psi_{\pm}(\tau)$. Figure 1(b) shows a typical realization of $x(t)$ for the exponential waiting times distribution in Fig. 1(c). We anticipate that the monotonicity of $\psi_{\pm}(\tau)$ prevents regular oscillations: it follows that the corresponding power spectral density S_x in Fig. 1(d) displays a Lorentzian-like shape. Figure 1(e), instead, shows a realization of the process $x(t)$ for the gamma-distributed waiting times reported in Fig. 1(f), which is characterized by a typical timescale for the switching mechanism. The power spectral density S_x of the process, shown in Fig. 1(g), features a pronounced peak at the typical frequency of the coherent oscillations. In both examples presented here, the average time $\langle \tau \rangle_{\pm}$ between two successive switches is large compared to relaxation time τ_{ν} , leading to the (almost) complete equilibration toward the two minima of the potential. In general, as we discuss below, the interplay between $\langle \tau \rangle_{\pm}$ and τ_{ν} determines qualitatively different types of stationary dynamics.

Dynamics.—We encode the state of the system at time t by the couple of stochastic variables $(x(t), \sigma(t))$, where $\sigma(t) = c(t)/c_0 = \pm 1$ is the sign of $c(t)$. A quantity of interest is the joint probability density $\rho_{\sigma}(x, t|x_0)$ for the system to be in the state (x, σ) at time t given that its initial state was $x(0) = x_0$. Its normalization requires $\sum_{\sigma} \int dx \rho_{\sigma}(x, t|x_0) = 1$ for all times $t \geq 0$. We derive a renewal equation for $\rho_{\sigma}(x, t|x_0)$, see Supplemental Material [47], in terms of the waiting-time distributions $\psi_{\sigma}(\tau)$ and of the probability density $G_{\sigma}^{(0)}(x, t|x_0)$. The latter is given

by the probability density to be in x at time t for an Ornstein-Uhlenbeck process with fixed center $c(t) = \sigma c_0$. From the formal expression of $\rho_{\sigma}(x, t|x_0)$, we determine the analytical expressions of the Laplace transform of the first and second moments of $x(t)$ for generic waiting-time distributions $\psi_{\sigma}(\tau)$.

Because switches break detailed balance, the system reaches a nonequilibrium stationary state at long times. For exponentially distributed waiting times with rates $r_{\sigma} = 1/\langle \tau \rangle_{\sigma}$, we find an explicit expression of the stationary distributions $\rho_{\sigma}^{\text{st}}(x) = \lim_{t \rightarrow \infty} \rho_{\sigma}(x, t|x_0)$. In this case, the finite-time densities $\rho_{\sigma}(x, t|x_0)$ satisfy Fokker-Planck equations with source terms

$$\partial_t \rho_{\sigma}(x, t|x_0) = -\partial_x J_{\sigma}(x, t) + r_{-\sigma} \rho_{-\sigma}(x, t|x_0) - r_{\sigma} \rho_{\sigma}(x, t|x_0), \quad (2)$$

where $J_{\sigma}(x, t) = -[\nu(x - \sigma c_0) + D \partial_x] \rho_{\sigma}(x, t|x_0)$ is the spatial probability current associated with particles in the state σ at time t . The stationary solutions $\rho_{\sigma}^{\text{st}}(x)$ of Eq. (2) are then given by

$$\rho_{\sigma}^{\text{st}}(x) = \frac{\mathcal{N}}{2} \int_{-1}^{+1} dz \rho_G(x - c_0 z) (1 - \sigma z)^{r_{\sigma}/\nu - 1} (1 + \sigma z)^{r_{-\sigma}/\nu}, \quad (3)$$

where we introduce the Gaussian distribution $\rho_G(x) \equiv \exp[-x^2 \nu / (2D)] / \sqrt{2\pi D / \nu}$. The constant $\mathcal{N}^{-1} \equiv \nu \sum_{\sigma} {}_2F_1(1, 1 - r_{-\sigma}/\nu, 1 + r_{\sigma}/\nu, -1) / r_{\sigma}$ guarantees the normalization of $\rho_{\sigma}^{\text{st}}(x)$, where ${}_2F_1$ is the hypergeometric

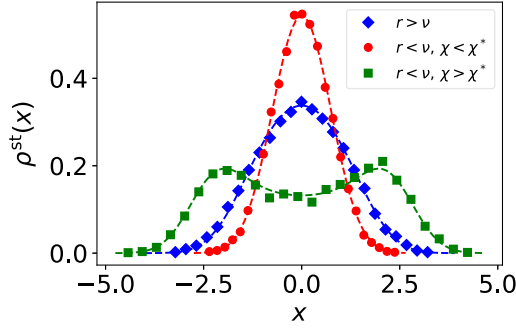


FIG. 2. Stationary probability density $\rho^{\text{st}}(x)$ for symmetric exponentially distributed waiting times: numerical simulations (symbols) are compared with the analytical solution in Eq. (3) (dashed lines). The three cases correspond to fixed values of $D = 1$ and $\nu = 2.5$, but various values of r and c_0 : blue, $c_0 = 2$ and $r = 5 > \nu$; red, $c_0 = 0.5$ and $r = 1.25 < \nu$, for which $\chi \simeq 0.31$; green, $c_0 = 2.5$ and $r = 1.25$, for which $\chi \simeq 7.8$. In the latter two cases, $\zeta = 1/2$ corresponding to the critical value $\chi^*(\zeta = 1/2) \simeq 1.58$ (see main text). The numerical estimates of $\rho^{\text{st}}(x)$ are obtained from $N = 10^4$ simulations of Eq. (1) using Euler's numerical integration method with time step $\Delta t = 5 \times 10^{-3}$.

function. Similar results were recently reported for run-and-tumble particles [48,49]. The total stationary density $\rho^{\text{st}}(x) = \rho_+^{\text{st}}(x) + \rho_-^{\text{st}}(x)$ can be either unimodal or bimodal, depending on the values of the parameters of the model, as shown in Fig. 2 numerically and analytically using Eq. (3). In particular, bistability emerges whenever the relaxation in the harmonic potential is fast enough with respect to the switching frequency and the amplitude of thermal fluctuations is small compared with the distance between the two minima of the potential. For symmetric and exponentially distributed waiting times, i.e., $r_\sigma = r$, we can characterize the transition from unimodal to bimodal analytically, exploiting the fact that $\rho^{\text{st}}(x)$ is unimodal if it displays a maximum at $x = 0$, and bimodal otherwise. The transition is controlled by the dimensionless parameters $\zeta \equiv r/\nu$, describing the interplay between relaxation and switching, and $\chi \equiv c_0^2\nu/(2D)$, which quantifies how much the two centers $\pm c_0$ are distinguishable with respect to the amplitude of thermal fluctuations. We find that for fast switching $r \geq \nu$ ($\zeta \geq 1$) the stationary distribution is always unimodal, as shown by the blue curve and data points in Fig. 2,

whereas for slow switching $r < \nu$ ($\zeta < 1$) $\rho^{\text{st}}(x)$ can display both mono- and bistability. In particular, the dynamics is monostable for $\chi \leq \chi^*(\zeta)$, as shown in red in Fig. 2, and bistable for $\chi > \chi^*(\zeta)$, shown in green. The critical value $\chi^*(\zeta)$ depends solely on ζ (see Supplemental Material [47]).

Another relevant quantity that characterizes the dynamics of the system is the long-time correlator $C_x(t) \equiv \lim_{\tau \rightarrow \infty} \langle x(t + \tau)x(\tau) \rangle$. Its Fourier transform is the power spectral density $S_x(\omega) = \hat{C}_x(\omega) = \langle |\hat{x}(\omega)|^2 \rangle$ [50], where we use the convention $\hat{f}(\omega) \equiv \int_{-\infty}^{+\infty} dt e^{-i\omega t} f(t)$ for the Fourier transform \hat{f} of a function f . Because the noise terms ξ and c in Eq. (1) are independent, it follows that

$$S_x(\omega) = \frac{2D + \nu^2 S_c(\omega)}{\nu^2 + \omega^2}, \quad (4)$$

where $S_c(\omega) = \langle |\hat{c}(\omega)|^2 \rangle$ is the power spectrum of $c(t)$. For generic non-Markovian $c(t)$, calculating $S_c(\omega)$ requires the knowledge of its stationary two-time statistics derived in the Supplemental Material [47]. In particular, the key quantity is the Laplace transform $\tilde{C}_c(s)$ of the long-time c correlator $C_c(t)$, defined as above, which is given by

$$\tilde{C}_c(s) = c_0^2 \left[\frac{1}{s} - \frac{2}{\langle \tau \rangle} \frac{\tilde{\Psi}_-(s)\tilde{\Psi}_+(s)}{1 - \tilde{\psi}_-(s)\tilde{\psi}_+(s)} \right]. \quad (5)$$

Here we define the Laplace transform of f as $\tilde{f}(s) \equiv \int_0^\infty dt e^{-st} f(t)$, thus $\tilde{\psi}_\sigma(s)$ and $\tilde{\Psi}_\sigma(s) = [1 - \tilde{\psi}_\sigma(s)]/s$ are, respectively, the transforms of the waiting-time distribution $\psi_\sigma(t)$ and of its cumulative $\Psi_\sigma(t) = \int_t^\infty d\tau \psi_\sigma(\tau)$, whereas $\langle \tau \rangle \equiv (\langle \tau \rangle_+ + \langle \tau \rangle_-)/2$ is the average half-period of the oscillations. The analyticity of $\tilde{C}_c(s)$ on the imaginary axis implies that $S_c(\omega) = \tilde{C}_c(i\omega) + \tilde{C}_c(-i\omega)$.

Recent works [51–54] revealed that nonmonotonic waiting-time distributions often emerge from underlying nonequilibrium stationary processes. These features may be described by gamma-distributed waiting times $\psi_\sigma(\tau) = [\theta_\sigma^{k_\sigma} \Gamma(k_\sigma)]^{-1} \tau^{k_\sigma-1} e^{-\tau/\theta_\sigma}$, with average $\langle \tau \rangle_\sigma = k_\sigma \theta_\sigma$ and Laplace transforms $\tilde{\psi}_\sigma(s) = (1 + s\theta_\sigma)^{-k_\sigma}$. For this example, the power spectrum $S_c(\omega)$ reads

$$S_c(\omega) = \frac{4c_0^2}{\langle \tau \rangle \omega^2} \frac{(R_+ R_-)^2 - 1 + (1 - R_-^2) R_+ \cos \phi_+ + (1 - R_+^2) R_- \cos \phi_-}{(R_+ R_-)^2 + 1 - 2R_+ R_- \cos(\phi_+ + \phi_-)}, \quad (6)$$

where we define $\phi_\sigma(\omega) \equiv k_\sigma \arctan(\omega\theta_\sigma)$ and $R_\sigma(\omega) \equiv (1 + \omega^2\theta_\sigma^2)^{k_\sigma/2}$. Equation (6) agrees with the numerical estimates of the power spectrum for both exponentially and gamma-distributed waiting times, as shown in Figs. 1(c) and 1(f), respectively. We find that the power spectrum

$S_x(\omega)$ displays a peak at a frequency ω_{max} for sufficiently large values of k , which depend on the choice of parameters. Moreover, for large values of k , the spectrum may display additional peaks close to the integer multiples of ω_{max} . For symmetric gamma-distributed waiting times,

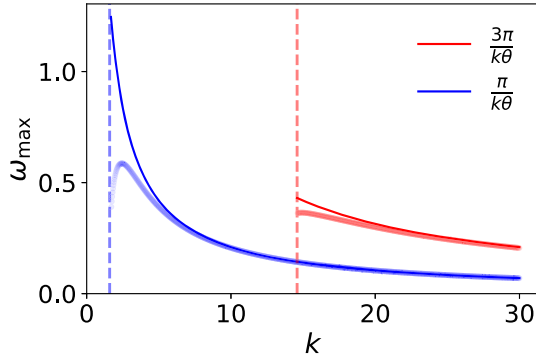


FIG. 3. Frequencies of the first (blue) and second (red) peaks of the power spectrum $S_x(\omega)$ in Eq. (4), as functions of k , for $\theta = 1.5$, $D = 0.5$, $c_0 = 1$, and $\nu = 2.5$. As k increases above ≈ 1.5 (dashed blue vertical line) a first local maximum appears in $S_x(\omega)$ at a typical frequency (blue symbols), well approximated by the blue solid line. As k exceeds ≈ 14.6 (dashed red vertical line), a second peak appears at a typical frequency (red symbols), well approximated by the red solid line.

Fig. 3 shows the frequencies corresponding to the first two peaks of $S_x(\omega)$ as a function of the shape parameter k . We note that the second peak appears for $k \gtrsim 14.6$ at frequency $\approx 3\omega_{\max}$, which results from the fact that, upon increasing k , $c(t)$ increasingly resembles a deterministic symmetric square wave whose Fourier spectrum has only odd harmonics.

Stochastic thermodynamics.—To characterize the thermodynamics of the active mechanism driving the oscillations, we evaluate the statistics of the work. The stochastic work $\delta W(t)$ [55] done on the system in the time interval $[t, t + dt]$ is given by $\delta W(t) = (\partial V / \partial c) \circ dc(t) = -\kappa x(t) \circ dc(t)$, where \circ denotes the Stratonovich product, and the second equality follows from $c^2(t) = c_0^2$. Note that $\delta W(t)$ is nonzero only when a switch occurs at time t : energy is injected into [extracted from] the system, i.e., $\delta W(t) > 0$ [$\delta W(t) < 0$], when $x(t)dc(t) < 0$ [$x(t)dc(t) > 0$]. From the analytical expression of the first moment of $x(t)$ at a switch, we derive the exact expression of the stationary average power $\langle \dot{W} \rangle = \lim_{t \rightarrow \infty} \langle \delta W(t) \rangle / dt$, i.e.,

$$\langle \dot{W} \rangle = \frac{2\kappa c_0^2 [1 - \tilde{\psi}_+(\nu)][1 - \tilde{\psi}_-(\nu)]}{\langle \tau \rangle [1 - \tilde{\psi}_+(\nu)\tilde{\psi}_-(\nu)]}, \quad (7)$$

which holds for *arbitrary* waiting-time distributions $\psi_\sigma(\tau)$. The average stationary power is always positive in agreement with the second law: $\langle \dot{W} \rangle = T \langle \dot{S}_{\text{tot}} \rangle \geq 0$, where $\langle \dot{S}_{\text{tot}} \rangle$ is the rate of entropy production. Moreover, Eq. (7) implies the upper bound $\langle \dot{W} \rangle \leq 2\kappa c_0^2 / \langle \tau \rangle$, which is saturated in the limit of infinitely fast relaxation time ($\nu \rightarrow \infty$). The upper bound $2\kappa c_0^2 / \langle \tau \rangle$ is the ratio between the characteristic energy $V_0 = \kappa(2c_0)^2/2$ that $x(t)$ fluctuating around the minimum of one potential acquires in the other potential immediately after the switch and the average time $\langle \tau \rangle$ between successive

switches. For $\nu \rightarrow \infty$, this V_0 is indeed the energy injected in the system at a switch. Furthermore, we derive in the Supplemental Material [47] exact expression of the average work $\langle W(t) \rangle = \int_0^t \langle \delta W(\tau) \rangle$.

Experimental application.—An example of a biological process displaying active oscillations is the spontaneous motion of hair bundles from a bullfrog’s ear [4,13,14]. The hair bundle is an organelle formed by a cohesive tuft of cylindrical stereocilia that protrude from the apical surface of the namesake hair cells. This receptor cells transduce a mechanical stimulus, such as a sound wave, into a neural signal and thus facilitates hearing and other sensory processes in vertebrates. The oscillatory motion of a hair bundle is powered by an active process, which is essential for the organelle’s sensory function, and results in the violation of the fluctuation-dissipation theorem [56].

Several stochastic models have been proposed for the time series of hair bundles [13,14,57–62]. All these models, which can be reduced to the family of Duffing–Van der Pol oscillators [13,33,35,36], rely on nonlinear equations of motion with hidden degrees of freedom of diverse origins. Under various conditions, such a system can describe both bistable and limit-cycle regimes of oscillatory motion, which are often not easy to distinguish.

In typical experiments, oscillating hair bundles display a great variety of different nonlinear oscillations [14]. We applied our theoretical model to symmetric bistable oscillations, and therefore we specifically select appropriate traces from our experimental recordings. These measurements were performed on a dissected mechanosensitive epithelium of a bullfrog’s sacculus, as described previously [63,64]. In an experiment, we mounted the mechanosensitive tissue in a two-compartment chamber, such that the hair cells were exposed to two different ionic solutions on their apical and basal side. This setup mimicked the physiological condition in which hair cells operate in the inner ear and evoked spontaneous oscillations of the hair bundles. To better resolve the movement of the oscillating hair bundle, we attached a glass fiber to the bundle’s tip and projected the shadow onto a photodiode [65]. This calibrated signal of the photodiode reported the position of the oscillating bundle as a function of time [blue line in Fig. 4(a)].

As reported below, the linear model proposed in this Letter is also capable of accounting for the basic features of the hair-bundle motion, which are common to simple active oscillators, see Figs. 4(a)–4(c). To make contact with the experimental data, we apply a simulation-based inference approach [66–68] (see Supplemental Material [47]) to determine values of the unknown parameters in Eq. (1) for a selection of three experimental cases, in which we observed simple symmetric oscillations of $x(t)$ in the case of gamma-distributed waiting times. Our model reproduces well the pattern of the hair-bundle motion as shown in Fig. 4(a). The simulated time series of $x(t)$ also

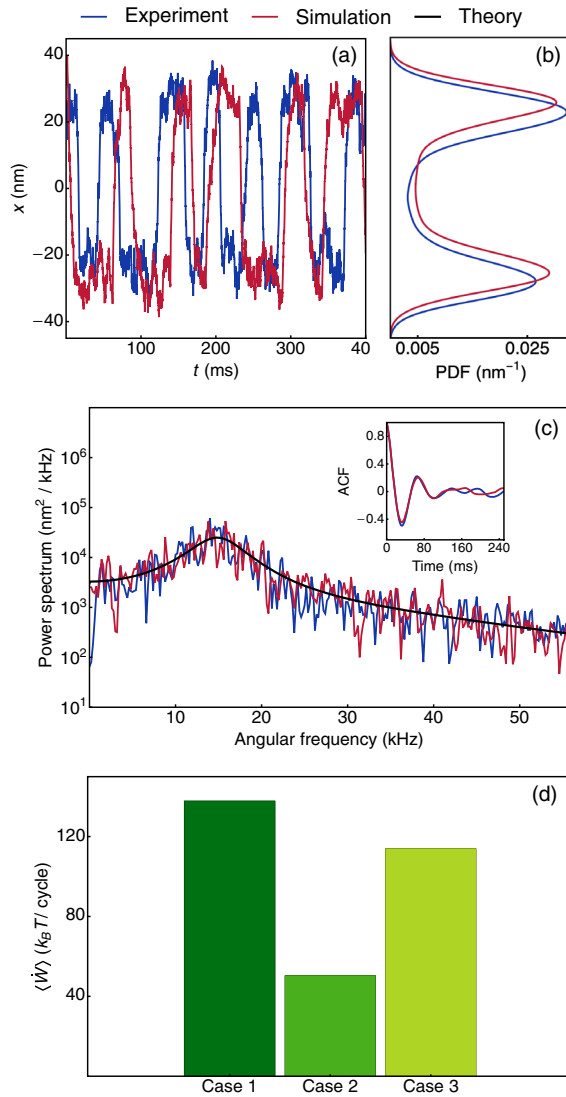


FIG. 4. Oscillations of a hair bundle’s tip $x(t)$ modeled by Eq. (1) in the case of symmetric gamma-distributed waiting times: experimental observations and simulations with inferred parameter values. (a) Example segments of experimental and simulated time series. (b) Probability density function (PDF) of $x(t)$. (c) Power spectrum of $x(t)$ with its autocorrelation function (ACF) shown in the inset. (d) Energy dissipated by hair bundles per one cycle in three experimental cases, see Table I in the Supplemental Material [47]. Only data of the experimental case 1 are shown in (a)–(c). Data for all the three cases are reported in the Supplemental Material [47].

quantitatively matches the probability density and time-frequency statistics of experimental measurements, see Figs. 4(b) and 4(c). Using the exact analytical predictions obtained for the equation of motion (1), we can estimate the average power dissipated by the active process that drives the hair-bundle oscillations in the bullfrog’s ear. Its value [Fig. 4(d)], $\langle \dot{W} \rangle \sim 100k_B T/\text{cycle}$, is of the same order of magnitude as estimates of the heat dissipation rate in the hair-bundle spontaneous fluctuations [56] and of the

viscous energy dissipation under weak, external periodic stimulation [69]. Assuming that active oscillations result from adenosine triphosphate (ATP) hydrolysis by myosin motors with a free energy change of $\sim 10k_B T$ per molecule [70], we estimate that about ten ATP molecules are required to fuel a single oscillation cycle of the hair bundle.

Discussion.—In this Letter, we have introduced an exactly solvable stochastic model describing the dynamics of non-Markovian active oscillators. This system displays key dynamical features of active oscillators: transition from a monostable to a bistable regime, sharp power spectra, broken detailed balance, and heat dissipation. We have also generalized the theoretical analysis presented here to accommodate asymmetric waiting-time distributions of the underlying noise (see Supplemental Material [47]), as observed in many biological processes [52]. We have also shown that our linear, non-Markovian model reproduces with high accuracy the probability density and power spectrum of several experimental recordings from the top of the bullfrog’s saccular hair bundle. Fitting the data to the model, we have calculated that the power consumption by the hair bundle during its spontaneous motion requires the consumption of at least ten ATP molecules per oscillation cycle. We expect that our model could be applied to decipher the energetics of other relevant active oscillations observed in living systems, such as confined cell migration [71], neuronal networks [72], and actomyosin gels [73].

R. G. A. was supported by Howard Hughes Medical Institute, of which A. J. H. is an Investigator. A. G. acknowledges support from MIUR PRIN project “Coarse-grained description for nonequilibrium systems and transport phenomena (CO-NEST)” Grant No. 201798CZL.

*gennaro.tucci@ds.mpg.de

†edgar@ictp.it

‡gambassi@sissa.it

§belousov.roman@gmail.com

- [1] K. Kruse and F. Jülicher, Oscillations in cell biology, *Curr. Opin. Cell Biol.* **17**, 20 (2005).
- [2] J. Toner, Y. Tu, and S. Ramaswamy, Hydrodynamics and phases of flocks, *Ann. Phys. (Amsterdam)* **318**, 170 (2005).
- [3] S. Ramaswamy, The mechanics and statistics of active matter, *Annu. Rev. Condens. Matter Phys.* **1**, 323 (2010).
- [4] A. Hudspeth, Integrating the active process of hair cells with cochlear function, *Nat. Rev. Neurosci.* **15**, 600 (2014).
- [5] J. Prost, F. Jülicher, and J.-F. Joanny, Active gel physics, *Nat. Phys.* **11**, 111 (2015).
- [6] M. E. Cates and J. Tailleur, Motility-induced phase separation, *Annu. Rev. Condens. Matter Phys.* **6**, 219 (2015).
- [7] C. Bechinger, R. Di Leonardo, H. Löwen, C. Reichardt, G. Volpe, and G. Volpe, Active particles in complex and crowded environments, *Rev. Mod. Phys.* **88**, 045006 (2016).
- [8] É. Fodor and M. C. Marchetti, The statistical physics of active matter: From self-catalytic colloids to living cells, *Physica (Amsterdam)* **504A**, 106 (2018).

- [9] M. Das, C.F. Schmidt, and M. Murrell, Introduction to active matter, *Soft Matter* **16**, 7185 (2020).
- [10] T. Demaerel and C. Maes, Active processes in one dimension, *Phys. Rev. E* **97**, 032604 (2018).
- [11] M. Shreshtha and R. J. Harris, Thermodynamic uncertainty for run-and-tumble-type processes, *Europhys. Lett.* **126**, 40007 (2019).
- [12] S. Cerasoli, S. Ciliberto, E. Marinari, G. Oshanin, L. Peliti, and L. Rondoni, Spectral fingerprints of non-equilibrium dynamics: The case of a Brownian gyrator, [arXiv:2201.04903](https://arxiv.org/abs/2201.04903).
- [13] P. Martin and A. Hudspeth, Mechanical frequency tuning by sensory hair cells, the receptors and amplifiers of the inner ear, *Annu. Rev. Condens. Matter Phys.* **12**, 29 (2021).
- [14] P. Martin, D. Bozovic, Y. Choe, and A. Hudspeth, Spontaneous oscillation by hair bundles of the bullfrog's sacculus, *J. Neurosci.* **23**, 4533 (2003).
- [15] R. Alonso, F. Goller, and G. B. Mindlin, Motor control of sound frequency in birdsong involves the interaction between air sac pressure and labial tension, *Phys. Rev. E* **89**, 032706 (2014).
- [16] E. Tang, J. Agudo-Canalejo, and R. Golestanian, Topology Protects Chiral Edge Currents in Stochastic Systems, *Phys. Rev. X* **11**, 031015 (2021).
- [17] C. Beta and K. Kruse, Intracellular oscillations and waves, *Annu. Rev. Condens. Matter Phys.* **8**, 239 (2017).
- [18] G. Buzsáki and A. Draguhn, Neuronal oscillations in cortical networks, *Science* **304**, 1926 (2004).
- [19] A. Cherevko, E. Bord, A. Khe, V. Panarin, and K. Orlov, The analysis of solutions behaviour of Van der Pol Duffing equation describing local brain hemodynamics, *J. Phys. Conf. Ser.* **894**, 012012 (2017).
- [20] A. Cherevko, A. Mikhaylova, A. Chupakhin, I. Ufimtseva, A. Krivoschapkin, and K. Y. Orlov, Relaxation oscillation model of hemodynamic parameters in the cerebral vessels, *J. Phys. Conf. Ser.* **722**, 012045 (2016).
- [21] R. FitzHugh, Impulses and physiological states in theoretical models of nerve membrane, *Biophys. J.* **1**, 445 (1961).
- [22] G. B. Mindlin, Nonlinear dynamics in the study of birdsong, *Chaos* **27**, 092101 (2017).
- [23] R. E. Mirollo and S. H. Strogatz, Synchronization of pulse-coupled biological oscillators, *SIAM J. Appl. Math.* **50**, 1645 (1990).
- [24] J. Nagumo, S. Arimoto, and S. Yoshizawa, An active pulse transmission line simulating nerve axon, *Proc. IEEE* **50**, 2061 (1962).
- [25] T. Nomura, S. Sato, S. Doi, J. P. Segundo, and M. D. Stiber, A Bonhoeffer–Van der Pol oscillator model of locked and non-locked behaviors of living pacemaker neurons, *Biol. Cybern.* **69**, 429 (1993).
- [26] A. C. Oates, L. G. Morelli, and S. Ares, Patterning embryos with oscillations: Structure, function and dynamics of the vertebrate segmentation clock, *Development* **139**, 625 (2012).
- [27] T. Roenneberg, E. J. Chua, R. Bernardo, and E. Mendoza, Modelling biological rhythms, *Curr. Biol.* **18**, R826 (2008).
- [28] K. Rompala, R. Rand, and H. Howland, Dynamics of three coupled Van der Pol oscillators with application to circadian rhythms, *Commun. Nonlinear Sci. Numer. Simul.* **12**, 794 (2007).
- [29] B. Van der Pol, Biological rhythms considered as relaxation oscillations, *Acta Med. Scand.* **103**, 76 (1940).
- [30] B. Van der Pol and J. Van der Mark, LXXII. The heartbeat considered as a relaxation oscillation, and an electrical model of the heart, *London, Edinburgh, Dublin Philos. Mag. J. Sci.* **6**, 763 (1928).
- [31] P. van Dijk and H. P. Wit, Amplitude and frequency fluctuations of spontaneous otoacoustic emissions, *J. Acoust. Soc. Am.* **88**, 1779 (1990).
- [32] G. Vettoretti and W. R. Peltier, Fast physics and slow physics in the nonlinear Dansgaard–Oeschger relaxation oscillation, *J. Clim.* **31**, 3423 (2018).
- [33] R. Belousov, F. Berger, and A. J. Hudspeth, Volterra-series approach to stochastic nonlinear dynamics: Linear response of the Van der Pol oscillator driven by white noise, *Phys. Rev. E* **102**, 032209 (2020).
- [34] S. Dago *et al.*, Virtual double-well potential for an underdamped oscillator created by a feedback loop, *J. Stat. Mech.* (2022) 053209.
- [35] R. Belousov, F. Berger, and A. Hudspeth, Volterra-series approach to stochastic nonlinear dynamics: The Duffing oscillator driven by white noise, *Phys. Rev. E* **99**, 042204 (2019).
- [36] D. Ó. Maoiléidigh, E. M. Nicola, and A. Hudspeth, The diverse effects of mechanical loading on active hair bundles, *Proc. Natl. Acad. Sci. U.S.A.* **109**, 1943 (2012).
- [37] J. Buceta, K. Lindenberg, and J. M. R. Parrondo, Stationary and Oscillatory Spatial Patterns Induced by Global Periodic Switching, *Phys. Rev. Lett.* **88**, 024103 (2001).
- [38] F. Müller-Hansen, F. Droste, and B. Lindner, Statistics of a neuron model driven by asymmetric colored noise, *Phys. Rev. E* **91**, 022718 (2015).
- [39] D. Huber and L. S. Tsimring, Dynamics of an Ensemble of Noisy Bistable Elements with Global Time Delayed Coupling, *Phys. Rev. Lett.* **91**, 260601 (2003).
- [40] Y. Yuzhelevski, M. Yuzhelevski, and G. Jung, Random telegraph noise analysis in time domain, *Rev. Sci. Instrum.* **71**, 1681 (2000).
- [41] R. Mankin, T. Laas, E. Soika, and A. Ainsaar, Noise-controlled slow–fast oscillations in predator–prey models with the Beddington functional response, *Eur. Phys. J. B* **59**, 259 (2007).
- [42] M. Kurzyński, Statistical properties of the dichotomous noise generated in biochemical processes, *Cell. Mol. Biol. Lett.* **13**, 502 (2008).
- [43] S. Gurvitz, A. Aharony, and O. Entin-Wohlman, Temporal evolution of resonant transmission under telegraph noise, *Phys. Rev. B* **94**, 075437 (2016).
- [44] A. Aharony, O. Entin-Wohlman, D. Chowdhury, and S. Dattagupta, Is telegraph noise a good model for the environment of mesoscopic systems?, *J. Stat. Phys.* **175**, 704 (2019).
- [45] S. Wittrock, P. Talatchian, M. Romera, M. J. Garcia, M.-C. Cyrille, R. Ferreira, R. Lebrun, P. Bortolotti, U. Ebels, J. Grollier, and V. Cros, Flicker and random telegraph noise between gyrotropic and dynamic C-state of a vortex based spin torque nano oscillator, *AIP Adv.* **11**, 035042 (2021).
- [46] M. Kac, A stochastic model related to the telegrapher's equation, *Rocky Mt. J. Math.* **4**, 497 (1974).

- [47] See Supplemental Material at <http://link.aps.org/supplemental/10.1103/PhysRevLett.129.030603> for the proof of the main results and more details on the data experimental analysis.
- [48] R. Garcia-Millan and G. Pruessner, Run-and-tumble motion in a harmonic potential: Field theory and entropy production, *J. Stat. Mech.* (2021) 063203.
- [49] A. Dhar, A. Kundu, S. N. Majumdar, S. Sabhapandit, and G. Schehr, Run-and-tumble particle in one-dimensional confining potentials: Steady-state, relaxation, and first-passage properties, *Phys. Rev. E* **99**, 032132 (2019).
- [50] N. G. Van Kampen, *Stochastic Processes in Physics and Chemistry* (Elsevier, New York, 1992).
- [51] Y. Tu, The nonequilibrium mechanism for ultrasensitivity in a biological switch: Sensing by Maxwell's demons, *Proc. Natl. Acad. Sci. U.S.A.* **105**, 11737 (2008).
- [52] D. J. Skinner and J. Dunkel, Estimating Entropy Production from Waiting Time Distributions, *Phys. Rev. Lett.* **127**, 198101 (2021).
- [53] I. A. Martínez, G. Bisker, J. M. Horowitz *et al.*, Inferring broken detailed balance in the absence of observable currents, *Nat. Commun.* **10**, 3542 (2019).
- [54] D. Hartich and A. Godec, Emergent Memory and Kinetic Hysteresis in Strongly Driven Networks, *Phys. Rev. X* **11**, 041047 (2021).
- [55] K. Sekimoto, Langevin equation and thermodynamics, *Prog. Theor. Exp. Phys.* **130**, 17 (1998).
- [56] É. Roldán, J. Barral, P. Martin, J. M. Parrondo, and F. Jülicher, Quantifying entropy production in active fluctuations of the hair-cell bundle from time irreversibility and uncertainty relations, *New J. Phys.* **23**, 083013 (2021).
- [57] Y. Choe, M. O. Magnasco, and A. Hudspeth, A model for amplification of hair-bundle motion by cyclical binding of Ca²⁺ to mechano-electrical-transduction channels, *Proc. Natl. Acad. Sci. U.S.A.* **95**, 15321 (1998).
- [58] J.-Y. Tinevez, F. Jülicher, and P. Martin, Unifying the various incarnations of active hair-bundle motility by the vertebrate hair cell, *Biophys. J.* **93**, 4053 (2007).
- [59] T. Reichenbach and A. Hudspeth, The physics of hearing: Fluid mechanics and the active process of the inner ear, *Rep. Prog. Phys.* **77**, 076601 (2014).
- [60] A. Vilfan and T. Duke, Two adaptation processes in auditory hair cells together can provide an active amplifier, *Biophys. J.* **85**, 191 (2003).
- [61] B. Cao, H. Gu, and K. Ma, Complex dynamics of hair bundle of auditory nervous system (I): Spontaneous oscillations and two cases of steady states, *Cogn. Neurodyn.* **1** (2021), [10.1007/s11571-021-09744-4](https://doi.org/10.1007/s11571-021-09744-4).
- [62] B. Cao, H. Gu, and R. Wang, Complex dynamics of hair bundle of auditory nervous system (II): Forced oscillations related to two cases of steady state, *Cogn. Neurodyn.* **1** (2021), [10.1007/s11571-021-09745-3](https://doi.org/10.1007/s11571-021-09745-3).
- [63] R. Alonso, M. Tobin, P. Martin, and A. Hudspeth, Fast recovery of disrupted tip links induced by mechanical displacement of hair bundles, *Proc. Natl. Acad. Sci. U.S.A.* **117**, 30722 (2020).
- [64] J. B. Azimzadeh and J. D. Salvi, Physiological preparation of hair cells from the sacculus of the American bullfrog (*Rana catesbeiana*), *J. Vis. Exp.* **121**, e55380 (2017).
- [65] J. B. Azimzadeh, B. A. Fabella, N. R. Kastan, and A. Hudspeth, Thermal excitation of the mechanotransduction apparatus of hair cells, *Neuron* **97**, 586 (2018).
- [66] A. Tejero-Cantero, J. Boelts, M. Deistler, J.-M. Lueckmann, C. Durkan, P. J. Gonçalves, D. S. Greenberg, and J. H. Macke, Sbi—a toolkit for simulation-based inference, *arXiv:2007.09114*.
- [67] G. Papamakarios and I. Murray, Fast ϵ -free inference of simulation models with Bayesian conditional density estimation, in *Advances in Neural Information Processing Systems 29 (NIPS 2016)* (2016), p. 1028, <https://proceedings.neurips.cc/paper/2016/hash/6aca97005c68f1206823815f66102863-Abstract.htm>.
- [68] J. Lueckmann, P. J. Gonçalves, G. Bassetto, K. Oecal, M. Nonnenmacher, and J. H. Macke, Flexible statistical inference for mechanistic models of neural dynamics, in *Neural Information Processing Systems 30 (NIPS 2017)* (2018), <https://proceedings.neurips.cc/paper/2017/hash/addfa9b7e234254d26e9c7f2af1005cb-Abstract.html>.
- [69] P. Martin and A. Hudspeth, Active hair-bundle movements can amplify a hair cell's response to oscillatory mechanical stimuli, *Proc. Natl. Acad. Sci. U.S.A.* **96**, 14306 (1999).
- [70] A. Hudspeth and P. G. Gillespie, Pulling springs to tune transduction: Adaptation by hair cells, *Neuron* **12**, 1 (1994).
- [71] D. B. Brückner, N. Arlt, A. Fink, P. Ronceray, J. O. Rädler, and C. P. Broedersz, Learning the dynamics of cell-cell interactions in confined cell migration, *Proc. Natl. Acad. Sci. U.S.A.* **118**, 1 (2021).
- [72] S. Nadkarni and P. Jung, Spontaneous Oscillations of Dressed Neurons: A New Mechanism for Epilepsy?, *Phys. Rev. Lett.* **91**, 268101 (2003).
- [73] P.-Y. Plaçais, M. Baland, T. Guérin, J.-F. Joanny, and P. Martin, Spontaneous Oscillations of a Minimal Actomyosin System under Elastic Loading, *Phys. Rev. Lett.* **103**, 158102 (2009).